For polymer composites, creep behavior is very important for practical application. There are some reports on the creep behaviors of polymer composites filled with inorganic particles [5–7]. For example, Yang et al. [8] carried out tensile creep tests on a few polyamide 66 composites filled with different nanoparticles. One of them was a composite with 1 wt% 21 nm TiO_2 particles modified with octylsilane. It was found that the creep resistance of nanocomposites was significantly enhanced by nanoparticles without sacrificing the tensile properties. Lietz et al. [9] investigated the mechanical properties and creep resistance of SBS block copolymers with nanoclay fillers and found that the introduction of dispersed nanoclays induced promising improvements in creep performance. Although surface modifications of nanofillers with organic chemicals are widely used [10–13], the effect of chemical connection between inorganic particle and organic matrix on creep behaviors was seldom found.

In this work, the microscopic variation mechanism of silane connection in silane–TiO_2/HDPE was investigated through compressive creep tests. Through the analysis of creep rate curves, the creep mechanisms were proposed, in which silane connection plays a key role. That is, upon loading silane connection supports load, stretches to relieve load and is finally broken by the concentrated stress.

Experimental procedures

Materials

Silane treated TiO_2/high-density polyethylene (silane–TiO_2/HDPE) composite was fabricated in Japan Fine Ceramics Center. The ratio of TiO_2 to HDPE is 40vol.%, with anatase mean particle size of 535 nm. TiO_2 powder was treated with silane-coupling agent of γ-MPS (γ[-(methacryloxy)propyl]trimethoxysilane) and mixed with HDPE. During the manufacturing process, kneading and compression molding was involved. The detailed manufacturing process was described in literature [3]. By the analysis of FTIR, it was confirmed that the surface of TiO_2 particles was connected with HDPE through formation of Ti–O–Si bonds.

Compressive creep

The specimens of silane–TiO_2/HDPE were cut to cylindrical shape and polished to diameter of 6 mm and height of 12 mm. A servo-hydraulic fatigue machine Model EHF-EB5 (Shimadzu Co. Ltd., Japan) was employed to carry out the tests. In compressive strength tests, the rate of displacement was maintained at 0.033 mm/s. Tests were carried out in air or in saline solution of 0.9% NaCl. The temperature was kept to be 25 °C in the two conditions. The temperature controlling of saline solution was realized by pumping and recycling the saline solution of 25 °C into the test trough during test process.

Morphology observation

For the tested samples, it is somewhat difficult to observe the fracture surfaces because friction of them during compressive process has blurred the fracture information. For explanation of the possible fracture mechanism, the outer side surfaces of tested specimens were observed by scanning electronic microscopy (SEM) Hitachi S-3000N. Prior to observation, the samples were cleaned ultrasonically and dried. Then the outer side surfaces were coated with Au to ensure clear images using Hitachi ion sputter E-1010. The layer thickness of Au coating is about 10 nm.

Results and discussion

Compressive properties

Compressive tests were performed in air and saline solution at room temperature for silane–TiO_2/HDPE. The compressive curves are shown in Fig. 1. The Young's moduli are 2.9 GPa in air and 2.1 GPa in saline solution. Compressive strengths are 71 MPa in air and 63 MPa in saline solution. Obviously, silane–TiO_2/HDPE is susceptible to saline solution, which resulted in lower Young's modulus and compressive strength.

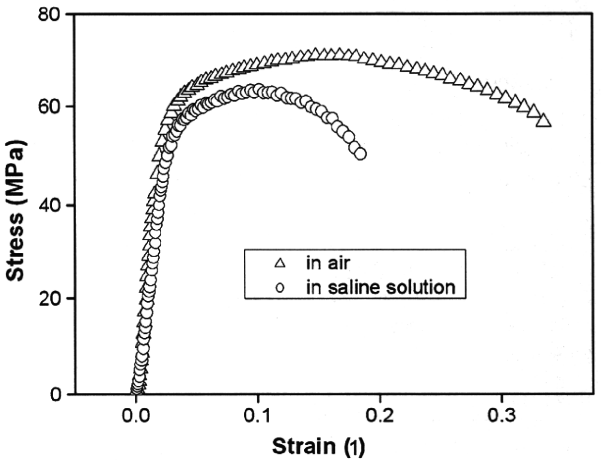

Fig. 1 Compressive stress–strain curves of silane–TiO_2/HDPE at room temperature in different surrounding conditions

Creep characterization

Creep deformability and stress dependence

The experimental curves of creep strain versus log time of silane–TiO_2/HDPE in air are presented in Fig. 2. The curves show that load stress has an important role on the creep behavior of silane–TiO_2/HDPE. With the increase of applied stress, the creep time to rupture becomes shorter and the dimensional deformation becomes larger.

The creep curve in saline solution at 45 MPa is shown in Fig. 3. As a comparison, the creep curve of air sample at the same stress level is also shown in the same figure. Creep life of silane–TiO_2/HDPE in saline solution is shortened greatly compared with that in air, while the creep strain remains almost the same. In other words, saline solution affected creep life greatly but had little influence on the dimensional stability.

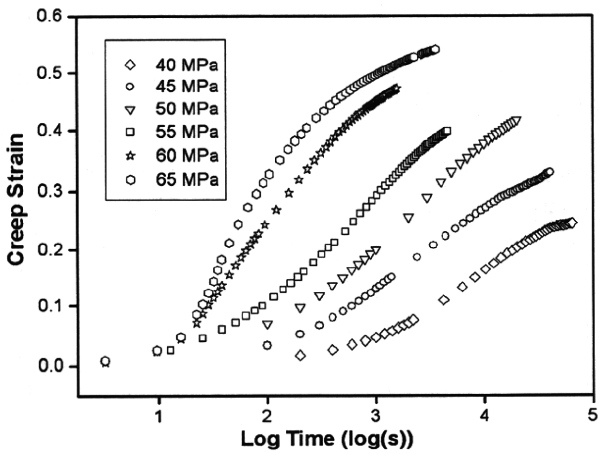

Fig. 2 Experimental creep curves of silane–TiO_2/HDPE in air under different stress levels

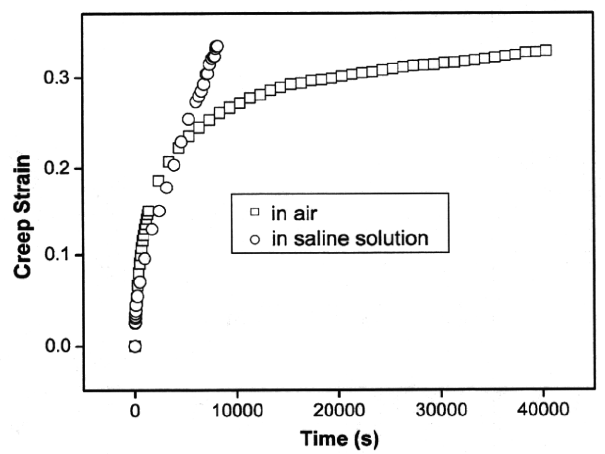

Fig. 3 Experimental creep curves obtained in saline solution and air under 45 MPa

Creep rate

The dimensional stability of materials is also determined by creep rate, which represents the velocity of creep deformation. The creep rate curves versus creep time under different stress levels are shown in Fig. 4. In air, the creep rate curves under stresses lower than 50 MPa all decrease with creep time monotonically. When the stress is higher than 50 MPa, the creep rates remain almost the same at the beginning. For 60 and 65 MPa, after almost 10 s, the creep rates increase sharply and soon come down. That is, all samples tested under different stresses only experienced the first primary creep stage, and did not attain the steady-state in the secondary stage. The creep rate at 45 MPa in saline solution is shown by the dash line. Clearly, the creep rate at the beginning is almost the same as that of 45 MPa in air, but it remains high creep rate for a while, then it decreases quickly and remains almost stable after 100 s. Furthermore, the creep rate at the instant of loading is increased with the load stress level before 50 MPa. After 50 MPa, it remains almost the same.

Outer side surface morphologies

As a comparison, Fig. 5 shows the outer side surface morphology of the original silane–TiO_2/HDPE sample before any test. The surface is very smooth with few exposed TiO_2 particles on it. However, for specimens tested under compressive strength and creep experiments in both air and saline solution, the observation with naked

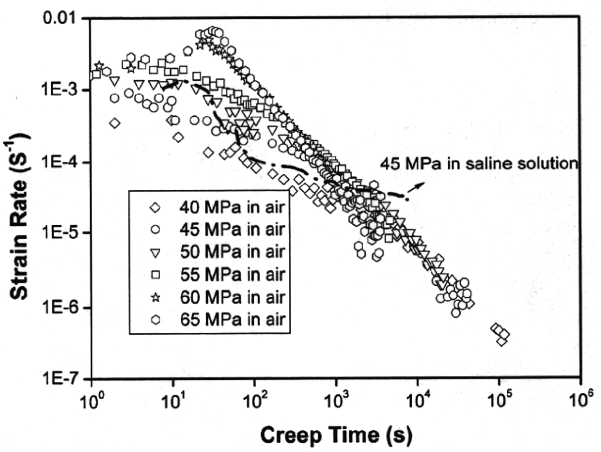

Fig. 4 Creep rate curves versus creep time at different stress levels

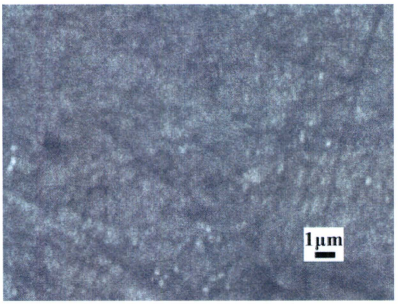

Fig. 5 Morphology of lateral surface of silane–TiO_2/HDPE specimen before any test

eyes and microscope showed that the cylindrical side surfaces (not the rupture surfaces) are covered with cracks and rugged areas, with only some differences in the general width of the cracks and the extent of coarseness between different experimental conditions. The surface coarsenesses of specimens tested in saline solution are severer than those in air. The representative cracks filled with broken crumbs are shown in Fig. 6. The side surface morphologies of the compressive samples are so complicated that only those that can contribute to the explanation of key problems are shown. To offer a clearer demonstration, the morphologies of would-be cracks or just rugged surfaces of high magnification are shown in Fig. 7. Although those samples were ultrasonically cleaned before SEM observation, the roughness and the number of exposed TiO_2 on their surfaces are obviously increased when compared with those of original specimen before any test. It is a common phenomenon for both air and saline solution samples experienced both compressive strength and creep testing. However, in Fig. 7a, deformed HDPE fibrils can be seen (shown by the arrows). These fibrils of HDPE were not found in other samples.

Creep mechanisms in air of silane–TiO_2/HDPE

Guild and Bonfield [14] by computer modeling showed that there are two regions of stress concentrations, one is the pole of the particle and the other is the interface. That is why so much work has been focused on the filler surface modification to reduce the stress concentrations. In silane–TiO_2/HDPE, the introduction of silane connection improved the interfacial compatibility effectively, but the interfacial failure still may be the reason for creep rupture.

Based on the variation of creep rates, creep mechanisms are proposed in Fig. 8. This schematic graph just exhibits a representative micro unit around a TiO_2 particle, which constitutes the whole bulk material. Silane-coupling agent has nine atoms along its main chain with some side chains like methyl, which inevitably resulted in the formation of voids and some unmodified surfaces on TiO_2. In order to squeeze those voids out and condense the material, kneading and compressing were employed during the manufacturing process. Therefore, the structure of this material before any load should be like Fig. 8a, in which the silane chains are entangled and curved on the surface of the particle. Once stress is loaded, the concentrated compressive stress on the interface will destroy the weak mechanical adhesion and be relaxed by stretching the silane chains in the perpendicular direction to the loading axis. Meanwhile the shear stress on the upper and the bottom of the particle surface, which is resulted from the small deformation and reorientation of silane chains, can also stretch other silane chains. The extent of stretching depends on the concentrated stress around the particle. Although under compressive stress the surrounding HDPE has to change in structure to help relieve stress concentrations, compared with silane chains during creep, deformation of HDPE and its effect on creep rate variation is

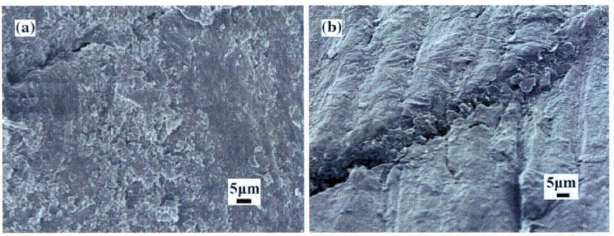

Fig. 6 Morphologies of lateral surfaces of specimens tested in **a** compressive experiment in saline solution; **b** compressive creep experiment in air at 55 MPa

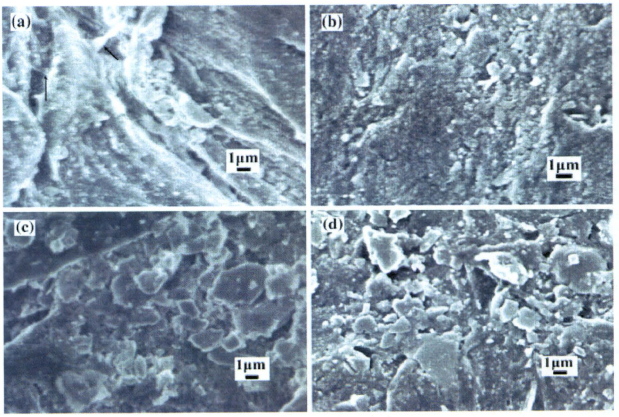

Fig. 7 Morphologies of lateral surfaces of specimens tested in **a** compressive strength experiment in air; **b** creep experiment in air under 55 MPa stress; **c** compressive strength experiment in saline solution; **d** creep experiment in saline solution under 45 MPa stress

negligible. So only the variation of silane chains is discussed here.

Imaginably, the variation extent of the silane chains is dependent on the load stress. From the creep rate curves, it is inferred that at the instant of loading, the loading energy can activate the silane chains even at 40 MPa. Between 40 and 50 MPa, with applied stress increased, the stretching extent is increased gradually without breaking of them (shown in Fig. 8b). Because the stretching process is not restricted within the stress range, the creep rate increases with the load stress at the instant of loading. When the stress reaches around 50 MPa, most of the load-bearing silane chains are stretched to their limitation (Fig. 8c). So at different stresses higher than 50 MPa, the creep rates all remain almost the same at the loading instant.

Accordingly, the destruction at the loading instant on structure is different. Below 50 MPa, the microstructure of silane–TiO_2/HDPE does not suffer obvious destruction. At 50 and 55 MPa, the silane chains are stretched to their limitation and maybe some of them are broken. The process is almost the same as the breakage in human femoral tissue. Acid phosphoprotein bonds connecting the non-calcified collagen fibril bands and the adjacent apatite crystals [4] were hypothesized to tend to weaken and eventually break when subjected to stress. When the stress reaches 60 MPa, most not all of the load-supporting silane chains are destroyed.

Once creep process starts, silane chains experience different process. At stresses lower than 50 MPa, they are pulled more straight gradually, which eventually results in their breakage. At 50 or 55 MPa, they begin to gradually break just after loading. At 60 MPa, although at the instant of loading, some of the silane chains are destroyed (depicted in Fig. 8d), the left still support. However, the left are also broken within short time, which resulted in the softness of bulk material exhibited by the increase of creep rate in Fig. 4. Because severe plastic deformation of composite is usually determined by the slippage between main chains of matrix, the subsequent reorientation hardness of HDPE slows down the creep rate.

Actually, the above discussion was made without considering the practical variation of sample external shape. For polymer composite, when compressed, the central lateral surface will protrude out with the reduction of axial length. With the increase of projection, tensile stress on the lateral surface will come into being and increase gradually. Just like the modeling of Bonfield [14], the tensile stress mainly concentrates on the interfaces between TiO_2 and HDPE and is released by the stretching and destruction of silane chains on the lateral surface of samples. Therefore, the above mentioned load-bearing silane chains at the instant of loading actually are those on the sample lateral surface. The stretching and destruction of silane connection begin from the sample outer surface and propagate gradually from the surface to the inner bulk sample.

The breakage of silane chains on sample surface can undoubtedly result in the initiation and propagation of cracks, which was proved by the morphologies shown in

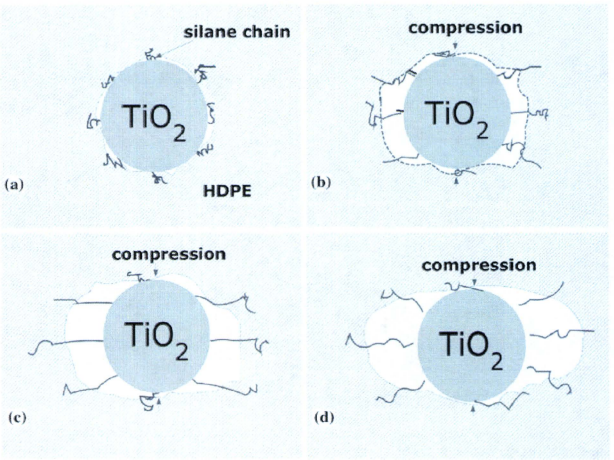

Fig. 8 Schematic graph of compressive creep mechanism **a** without any loading; **b** when load stress lower than 50 MPa; **c** when load stress higher than 50 MPa; **d** almost all the silane chains broken by compressive loading

Fig. 6. From the surface morphologies, the creep failure should be dominated by micorcrack failure mechanism for all the tested samples. Besides the microcrack failure mechanism, ductile failure on HDPE also competes with it, which can be manifested by the coexistence of HDPE fibrils and the exposed TiO_2 in Fig. 7a. Because the creep time to failure in the compressive strength experiment in air was the shortest (about 8 s), it was not enough for the silane connection at the interfaces to react and relieve the loading, so some of the concentrated stress was relieved by the deformation of HDPE directly. When the creep time was enough long or the creep happened in saline solution, interfacial failure mechanism defeated the ductile failure on matrix completely.

Effect of saline solution

It has been proved that biomaterial silane–TiO_2/HDPE is waterproof. When it was placed in saline solution for 2 days without any loading, its weight did not change. It is inferred that the effect of saline solution is synergetic with loading and from sample surface.

The interfacial failures in both air and saline solution are actually microcrack failure process. That is, after the breakage of silane chains at the interfaces, microcracks initiate, propagate, develop into main crack and finally result in the final failure. From the exposed TiO_2 particles in the surface morphology pictures, it is believed that the breakage is from Ti–O–Si bonds. Because of the hydrophilicity of TiO_2 surface, the basis for its bioactivity in biomaterials [15], once stress concentrations on sample surface are enough to break the chemical bond of Ti–O–Si, Ti–OH and Si–OH will form subsequently. In air, the forming process is very slow, while in saline solution, the process is sped up because of the surrounding water. The steric hindrance and repelling force between hydrogen atoms from the introduced –OH in air and the additional hydrostatic force and steric hindrance from water in saline solution all can enhance the stress concentrations in return. Because the tensile stress on lateral surface of samples was increased gradually with creep process, the effect of saline solution on creep rate should be time-dependent. It is very small at creep beginning and becomes gradually remarkable after that, which is the reason for the almost same creep rate at the creep beginning and comparatively higher creep rate after that when compared with the creep rate in air at the same stress level in Fig. 3.

From the creep mechanism at 45 MPa described above, it is known that under compressive load, those load-supporting silane chains stretches to their full length and then are broken gradually. The stretching and breakage of silane chains dominates the whole creep failure process. The sample in saline solution experienced the same failure process as that of air sample at the same stress level only with accelerated speed. Therefore, the total strain at break of sample tested in saline solution is almost the same as

that in air at 45 MPa, which is in consistency with the creep mechanisms proposed above.

Conclusions

To explore whether silane chains in silane–TiO_2/HDPE has the same function as phosphoprotein bonds in natural bones, the compressive creep tests of biomaterial silane–TiO_2/HDPE were carried out in both air and saline solution. The intense silane connection played a very important role in the creep process. That is, upon loading, silane chains supported the stress firstly, stretched to relieve the concentrated stress and then were broken. The creep failure process is microcrack initiation mechanism for both air and saline solution samples with only the difference of accelerated failure speed in saline solution. The susceptibility of silane–TiO_2/HDPE to environmental saline solution comes from the hydrophilicity of TiO_2 surface. The time-dependent effect of saline solution on the creep process and almost same total creep strain in saline solution as that of sample tested in air at the same stress level proved the proposed creep mechanisms.

References

1. Bonfield W, Grynpas MD, Tully AE, Bowman J, Abram J (1981) Biomaterials 2:185
2. Takadama H, Hashimoto M, Takigawa Y, Mizuno M, Kokubo T (2004) Key Eng Mater 254–256:569
3. Hashimoto M, Takadama H, Mizuno M, Kokubo T (2006) Mater Res Bull 41:515
4. Ascenzi M, Comite MD, Mitov P, Kabo JM (2007) J Biomech 40:2619
5. Pegoretti A, Kolarik J, Peroni C, Migliaresi C (2004) Polymer 45:2751
6. Zhang Z, Yang J-L, Friedrich K (2004) Polymer 45:3481
7. Xia H, Song M, Zhang Z, Richardson M (2007) J Appl Polym Sci 103:2992
8. Yang J-L, Zhang Z, Schlarb AK, Friedrich K (2006) Polymer 47:2791
9. Lietz S, Yang J, Bosch E, Sandler JKW, Zhang Z, Altstädt V (2007) Macromol Mater Eng 292:23
10. Zhou TH, Ruan WH, Yang JL, Rong MZ, Zhang MQ, Zhang Z (2007) Compos Sci Technol 7:2297
11. Tee DI, Mariatti M, Azizan A, See CH, Chong KF (2007) Compos Sci Technol 67:2584
12. Othman N, Ismail H, Mariatti M (2006) Polym Degrad Stab 91:1761
13. Zhang SM, Liu J, Zhou W, Cheng L, Guo XD (2005) Curr Appl Phys 5:516
14. Guild FJ, Bonfield W (1998) J Mater Sci Mater Med 9:497
15. Mohamed KR, Mostafa AA (2008) Mater Sci Eng C 28:1087

Review

Journal of Photopolymer Science and Technology
Volume23,Number2(2010)161 – 166©2010CPST

Photo-induced Functionalization on Biomaterials Surfaces

Kazuhiko Ishihara and Masayuki Kyomoto
Department of Materials Engineering, Department of Bioengineering,
7-3-1, Hongo, Bunkyo-ku, Tokyo 113-8656, Japan
and
Core Research Evolutional Science and Technology (CREST)
Japan Science and Technology Agency (JST)
5 Sanban-cho, Chiyoda-ku, Tokyo 102-0075, Japan
ishihara@mpc.t.u-tokyo.ac.jp

We reported the fabrication of a highly hydrophilic nanometer-scale modified surface on the inert polymer substrate by photo-induced graft polymerization of 2-methacryloyloxyethyl phosphorylcholine (MPC) to obtain biocompatible surfaces. As substrates, poly(ether-ether-ketone) (PEEK) were used. Photoinduced radical formation on the substrate could be realized without any photosensitizer because of the benzophenone units in PEEK molecular structure, which acts as a photo-initiator during the graft polymerization. The poly(MPC)(PMPC)-grafted PEEK surface fabricated by a novel and simple polymerization system exhibited unique characteristics such as high wettability and high anti-protein adsorption, which makes it highly suitable for medical applications.
Keywords: poly(ether-ether-ketone), self-initiated photopolymerization, biomaterials

1. Introduction

Surface modification is one of the most important technologies for the preparation of new multifunctional biomaterials for satisfying several requirements; surface modifications used today include coating, blending, and grafting. In general, graft polymerization is performed most frequently using either of the following methods that utilize chemical and/or physical processes: (a) surface-initiated graft polymerization or "grafting from" methods in which the monomers are polymerized from initiators or comonomers, and (b) adsorption of the polymer to the substrate or "grafting to" methods, such as reaction of the end groups of the ready-made polymers with the functional groups of the substrate. The "grafting from" method has an advantage over the "grafting to" method wherein it forms a high-density polymer brush interface with a multifunctional polymer; this advantage proves to be functionally effective.

When the benzophenene (BP) is exposed to photo-irradiation such as ultraviolet-ray (UV)-irradiation, a pinacolization reaction is induced; this results in the formation of semi-benzopinacol radicals (i.e., ketyl radicals) that act as photo-initiators. Therefore, in this study, we have focused upon a BP unit in PEEK and formulated a self-initiated surface-graft polymerization method that utilizes the BP unit in graft-from polymerization (Fig. 1).

2-Methacryloyloxyethyl phosphorylcholine (MPC), a methacrylate monomer bearing a phosphorylcholine group, is used to synthesize polymer biomaterials having excellent biocompatibility [1-3]; the MPC polymers have potential applications in a variety of fields such as biomedical science, surface science, and

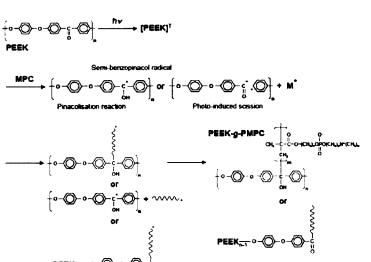

Fig. 1 Scheme for photo-induced polymerization of MPC on PEEK substrate.

Received March 31, 2010
Accepted May 7, 2010

bioengineering because they possess unique properties such as excellent antibiofouling, and low friction abilities. Thus, surface modification with the MPC polymer on medical devices is effective for obtaining biocompatibility.

In this review, we have demonstrated the fabrication of a biocompatible and highly hydrophilic nanometer-scale-modified surface by poly(MPC) (PMPC)-grafting onto the self-initiated PEEK surface using a photo-induced reaction; further, we also investigated the effects of photo-irradiation time and MPC concentration variability on PMPC-graft polymerization [4, 5]. The results revealed that it was possible to control the PMPC-graft layer in order to improve wettability, lubricity, and anti-protein adsorption for developing multifunctional PEEK biomaterials.

2. Materials and methods

2.1. Self-initiated Graft Polymerization of MPC

The preparation of PMPC-grafted PEEK is schematically illustrated in Fig. 1. PEEK specimens were machined from an extruded PEEK (450G; Victrex PLC, Thornton-Cleveleys, UK) bar stock, which was fabricated without stabilizers or additives. The surfaces of the PEEK specimens were ultrasonically cleaned in ethanol for 20 min, and then dried in vacuum. MPC was synthesized using the method reported by Ishihara et al. [6]. It was dissolved in degassed water to obtain 0.25- and 0.50-mol/L MPC aqueous solutions, and PEEK specimens were immersed in these solutions. Photo-induced graft polymerization was carried out at 60°C for 5–90 min on the PEEK surface under UV-irradiation (UVL-400HA ultra-high pressure mercury lamp; Riko-Kagaku Sangyo Co. Ltd., Funabashi, Japan) with an intensity of 5 mW/cm^2; a filter (model D-35; Toshiba Corp., Tokyo, Japan) was used to restrict the passage of UV-light to wavelengths of 350 ± 50 nm. After polymerization, the PMPC-grafted PEEK specimens were removed from the reaction solution, washed with pure water and ethanol to remove non-reacted monomers and non-grafted polymers, and dried at room temperature.

2.2. Surface Analysis of PMPC-grafted PEEK

The functional group vibrations of the PMPC-grafted PEEK surfaces were examined by Fourier-transform infrared (FT-IR) spectroscopy with attenuated total reflection (ATR) equipment. The FT-IR/ATR spectra were obtained using an FT-IR analyzer (FT/IR615; JASCO Co. Ltd., Tokyo, Japan) for 32 scans over the range of 1000–1800 cm^{-1} at a resolution of 4.0 cm^{-1}.

The surface elemental conditions of the PMPC-grafted PEEK surfaces were analyzed by X-ray photoelectron spectroscopy (XPS). The XPS spectra were obtained using an XPS spectrophotometer (AXIS-HSi165; Kratos/ Shimadzu Co., Kyoto, Japan) equipped with a 15-kV Mg-Ka radiation source at the anode. The take-off angle of the photoelectrons was maintained at 90°. Five scans were taken for each sample.

The static-water contact angles on the PMPC-grafted PEEK surfaces were measured by the sessile drop method using an optical bench-type contact angle goniometer (Model DM300; Kyowa Interface Science Co. Ltd., Saitama, Japan). Measurements were repeated fifteen times for each sample, and the average values were regarded as the contact angles.

2.3. Mechanical Test

The mechanical properties of untreated PEEK and PMPC-grafted PEEK with a 0.50-mol/L MPC concentration and 90-min photo-irradiation time were evaluated with tensile and flexural tests. Tensile testing was performed according to ISO527 standard using a type 1B tensile bar specimen and a crosshead speed of 50 mm/min. Flexural testing was performed according to ISO178 standard with a crosshead speed of 2 mm/min. The results derived from each measurement in the mechanical test were expressed as the mean values ± standard deviation. The statistical significance ($p < 0.05$) was estimated by Student's *t*-test.

2.4. Characterization of Protein Adsorption by Micro-bicinchoninic Acid Method

The amount of protein adsorbed on the PMPC-grafted PEEK surfaces was measured by the micro-bicinchoninic acid (BCA) method. Each specimen was immersed in Dulbecco's phosphate-buffered saline (PBS, pH 7.4, ion strength = 0.15 M; Immuno-Biological Laboratories Co. Ltd., Takasaki, Japan) for 1 h to equilibrate the PMPC-grafted surface. The specimens were immersed in bovine serum albumin (BSA, Mw = 6.7 × 10^4; Sigma-Aldrich Corp., MO, USA) solution at 37°C for 1 h. The protein solution was prepared in a BSA concentration of 4.5 g/L, i.e., 10% of the concentration of human plasma levels. Then, the specimens were rinsed five times with fresh PBS and immersed in 10.0-g/L sodium dodecyl sulfate (SDS) aqueous solution and shaken at room

temperature for 1 h to completely detach the adsorbed BSA on the PMPC-grafted surface. A protein analysis kit (micro BCA protein assay kit, #23235; Thermo Fisher Scientific Inc., IL, USA) based on the BCA method was used to determine the BSA concentration in the SDS solution, and the amount of BSA adsorbed on the PMPC-grafted PEEK surface was calculated.

3. Results

FT-IR/ATR spectra of untreated PEEK and PMPC-grafted PEEK with a 0.50-mol/L MPC concentration and 90-min photo-irradiation time shows transmission absorption peaks were observed at 1600, 1490, 1280, 1190, and 1160 cm^{-1} for both untreated PEEK and PMPC-grafted PEEK. These peaks are chiefly attributed to the diphenyl ether group, phenyl rings, or aromatic hydrogens in the PEEK substrate [7]. However, absorption peaks at 1720 and 1080 cm^{-1} (shoulder peak) were observed only for PMPC-grafted PEEK. These peaks corresponded to the carbonyl group (C=O) and phosphate group (P–O) in the MPC unit, respectively [8]. The XPS spectra of the binding energy region of the nitrogen (N) and phosphorous (P) electrons showed peaks for untreated PEEK and PMPC-grafted PEEK, whereas, peaks were not

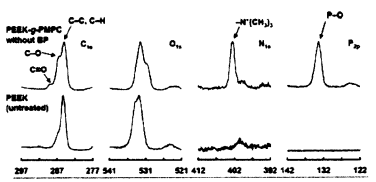

Fig. 2. XPS spectra of PEEK and PMPC-grafted PEEK.

observed in the case of untreated PEEK. The peaks at 403 and 134 eV were attributed to the $-N^{+}(CH_3)_3$ and phosphate groups, respectively. These peaks indicate the presence of phosphorylcholine in the MPC units. After PMPC grafting, the peaks attributed to the MPC unit were clearly observed in both the FT-IR/ATR and XPS spectra of the PMPC-grafted PEEK. These results indicate that PMPC was successfully grafted on the PEEK surface.

Fig. 3 shows the N and P concentrations of the PMPC-grafted PEEK as a function of the photo-irradiation time during polymerization at 0.25- and 0.50-mol/L MPC concentrations. The N and P concentrations increased with the photo-irradiation time. When the photo-irradiation time was shorter than 45 min, the N and P concentrations of the PMPC-grafted PEEK surface with a 0.50-mol/L MPC concentration were higher as compared with those with a 0.25-mol/L MPC concentration. The N and P concentration in the PMPC-grafted PEEK with both 0.25- and 0.50-mol/L MPC concentrations increased to 5.2 up to a photo-irradiation time of 90 min; those values were almost equivalent to the theoretical elemental composition (N = 5.3, P = 5.3) of PMPC. These results indicate that the PMPC layer fully covered the surface of the PEEK substrate.

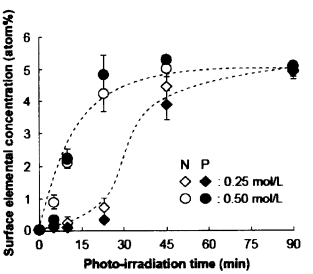

Fig. 3. Surface elemental concentration on PMPC-graft PEEK as a function of photo-irradiation time.

The physical properties of PMPC-graft layer on the PEEK surface as a function of the photo-irradiation time at MPC concentrations of 0.25 and 0.50 mol/L was evaluated. The PMPC-graft layer density of the PMPC-grafted PEEK with 0.25-mol/L MPC concentrations increased proportionally to 2.3 g/cm^3 with the photo-irradiation time. In the case of PMPC-grafted PEEK obtained with 0.50-mol/L MPC concentrations, the PMPC-graft layer density rapidly increased to 1.3 g/cm^3 up to a photo-irradiation time of 10 min; it then increased slowly to 2.2 g/cm^3 with an increase in the photo-irradiation time.

The mechanical properties of untreated PEEK and PMPC-grafted PEEK are summarized in Table 1. Tensile properties and flexural modulus did not differ significantly ($p > 0.05$) between untreated PEEK and PMPC-grafted PEEK. In contrast, there was a small but significant difference ($p < 0.05$) in the flexural strength and strain of untreated PEEK

Table 1. Mechanical property of PMPC-grafted PEEK.

Test method	Property	PEEK (untreated)	PMPC-grafted PEEK	t-Test
Tensile test	Yield strength (MPa)	109.4 (0.4)*	109.9 (0.6)	N.S.
	Ultimate strength (MPa)	71.5 (1.5)	71.7 (1.7)	N.S.
	Elongation (%)	24.0 (9.5)	24.4 (9.0)	N.S.
Flexural test	Ultimate strength (MPa)	168.9 (0.6)	173.7 (1.8)	< 0.05
	Ultimate strain (%)	8.4 (0.1)	6.7 (0.2)	< 0.05
	Modulus (GPa)	3.9 (0.0)	3.9 (0.0)	N.S.

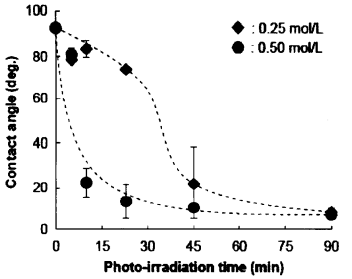

Fig. 4. Static contact angle by water on PMPC-grafted PEEK as a function of photo-irradiation time.

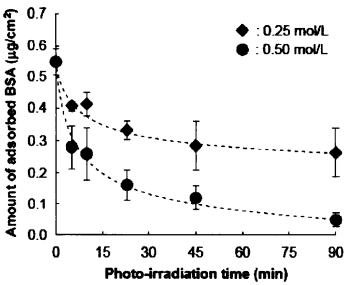

Fig. 5. Protein adsorption on PMPC-grafted PEEK as a function of photo-irradiation time.

and PMPC-grafted PEEK examined in this study. However, both untreated PEEK and PMPC-grafted PEEK met the ASTM F2026 requirements.

Fig. 4 shows the static-water contact angle of PMPC-grafted PEEK obtained with MPC concentrations of 0.25 and 0.50 mol/L as a function of the photo-irradiation time. The static-water contact angle of untreated PEEK was 90° and decreased markedly with an increase in the photo-irradiation time. When the photo-irradiation time was 90 min, the static-water contact angle of PMPC-grafted PEEK was the lowest value at <10°.

Fig. 5 shows the amount of protein (BSA) adsorbed on PMPC-grafted PEEK as a function of the photo-irradiation time with MPC concentrations of 0.25 mol/L and 0.50 mol/L. The amount of adsorbed BSA of PMPC-grafted PEEK decreased remarkably with an increase in photo-irradiation time.

4. Discussion

We demonstrated the fabrication of a biocompatible and highly hydrophilic nanometer-scale-modified surface by PMPC-grafting onto the self-initiated PEEK surface using a photo-induced grafting-from polymerization reaction, i.e., "self-initiated surface graft polymerization." The following methods were employed in our study: (a) grafting from polymerization for the formation of a high-density graft polymer layer, (b) photo-induced polymerization in the absence of photo-initiators, and (c) using biocompatible hydrophilic macromolecules, which exhibited photo-reduction by H-abstraction of a BP unit in PEEK from an H-donor; this induced surface-initiated graft polymerization of the feed methacrylate-type monomer (i.e., MPC) on the PEEK surface, even in the absence of a photo-initiator such as BP.

It is important to control the thickness and density of graft polymer layer for optimizing several areas of applications, e.g., in adhesion, colloid stabilization, and lubrication. When the photo-irradiation time was greater than 45 min, the PMPC-graft layer thicknesses became almost constant. Moreover, at the same photo-irradiation time of 90 min, it was shown that the higher the monomer concentration, the thicker the graft layer obtained: the PMPC-graft layer thickness (approximately 100 nm) of the PMPC-grafted PEEK obtained with 0.50-mol/L MPC concentration was thicker than that (approximately 40 nm) with 0.25-mol/L MPC concentration. The phenomenon can be attributed to the fact that the graft layer thickness increases with monomer concentration. When the PMPC layer has a brush-like structure, the graft layer thickness may correlate with the molecular weight of the grafted PMPC. The high-density PMPC-graft layer on the PEEK surface is assumed to exhibit a brush-like structure [9, 10]. It is generally well known that the reaction rate of radical polymerization is extremely high [11]. It was observed that the graft layer thickness (i.e., molecular weight of the graft polymer) was greatly

dependent on the monomer concentration, but virtually independent of the photo-irradiation time. Thus, in this study, the length (molecular weight) of the PMPC-graft chains was assumed to be successfully controlled by the MPC concentration used for polymerization. This indicates that the length of the PMPC chain grafted on the PEEK surface increased with the MPC concentration during polymerization [12]. Additionally, a uniform PMPC layer was clearly observed on the surface of the PEEK substrate, and no cracks or delaminating were observed at the PEEK substrate or the interface between the PMPC layer and PEEK substrate. These results indicate that the PMPC layer formed on the PEEK substrate is uniformly distributed over the substrate and is bound to the substrate by covalent C–C bonds.

On the other hand, the PMPC-graft layer density on the PEEK surface almost linearly increased to >2.2 g/cm^3 with the photo-irradiation time, suggesting that the graft chain propagates steadily with increasing photo-irradiation time. In order to obtain the high-density PMPC-graft layer, the photo-irradiation time must be controlled. Further, interestingly, while using an MPC concentration of 0.50 mol/L, the rate of the increase in the PMPC-graft layer density was low with a photo-irradiation time above 10 min. The present self-initiated surface graft polymerization method is photo-induced by UV-irradiation onto the BP unit of PEEK surface. In this study, it is assumed that the UV-irradiation directly produces a high-concentration free radical, because this PEEK is a semi-crystalline structure (crystalline, 30–40%) with a high-density BP unit in the surface. When the MPC concentration in a feed is also high, the self-initiated surface graft polymerization between the radicals on the PEEK surface and the MPC occurs extremely rapidly in the reaction system, forming the high-density graft chain on the surface. Hence, diffusion of the MPC monomer onto the PEEK surface might be interfered by the high-density graft chain because of its high viscosity. When the monomers attached to the PEEK surface were subjected to UV-irradiation, radicals were freely formed on the PEEK surface in the early stage but not in the late stage of polymerization, probably because the high-density grafted polymer chains formed by then blocked the diffusion of the monomer to the PEEK surface. Therefore, it is supposed that the rate of increase in the PMPC-graft layer density changed due to the high concentration of free radicals and monomers.

The wettability by water of the PMPC-grafted PEEK surface is considerably greater than that of the untreated PEEK surface (Fig. 4), because of the presence of a nanometer-scaled PMPC layer: MPC is a highly hydrophilic compound, while PMPC is water-soluble. We also observe that the dynamic coefficient of friction was greatly dependent on the water-wettability (static-water contact angle), but virtually independent of the structure (thickness and density) of the graft layer. A significant reduction in the static-water contact angle of the PMPC-grafted surface resulted in a substantial improvement in friction property. Fluid-film lubrication (or hydration lubrication) with the PMPC-grafted surface was achieved by the intermediate hydrated layer. It can be affirmed that this highly lubricated surface utilizing PMPC mimics the natural cartilage structure [13]. When the PEEK surface is modified by PMPC-grafting, the grafted PMPC causes a significant reduction in sliding friction between the graft surfaces because the thin water films that are formed act as extremely efficient lubricants. The water-lubrication systems utilizing PMPC suppress direct contact of the counter-bearing face with the PEEK substrate in order to reduce the frictional force. Thus, the PMPC-graft layer is expected to significantly increase the durability of the bearing biomaterials.

The fabrication of surfaces that exhibit anti-protein adsorption and/or cell adhesion has been one of goals of surface engineering for medical devices. The adsorption of the BSA on the PMPC-grafted PEEK surface decreased to 10% ($p < 0.001$) with an increase in photo-irradiation time, as shown in Fig. 5, as compared to that in untreated PEEK. It is shown that the extent of protein rejection is related to the PMPC-graft extent. Extensive grafting gives rise not only to an increase in the thickness of graft layer but also to an increase in the volume fraction (i.e., density) of graft segments in the layer. Therefore, it was thought that these characteristics of thickness and density of the PMPC-graft layer had a significant influence on protein adsorption. The mechanism of protein adsorption resistance on the PMPC-grafted surface is hypothesized as follows: the protein adsorption resistance attributed to the water-fluid film and hydration layer was due to water and hydrophilic macromolecules with volume exclusion effects. The presence of the water-fluid film and hydration layer is responsible for the easy detachment of proteins and the prevention of conformational changes in the adsorbed proteins. These results

imply that the PMPC-grafted PEEK surface is biocompatible in terms of tissue and blood compatibility, because MPC polymer-modified surfaces are known to exhibit *in vivo* antibiofouling.

As shown in Table 1, the mechanical properties of the PEEK are unchanged even after PMPC-grafting. This indicates that the photo-induced radical graft polymerization proceeds only on the surface of the PEEK substrate, while the properties of the substrate remain unchanged. Retention of the properties of the PEEK substrate is very important in clinical use, because the biomaterials used in implants act not only as surface-functional materials but also as structural materials *in vivo*.

The design of a well-characterized surface is a considerably important and difficult task. The photo-induced graft polymerization in the absence of photo-initiators of this study, i.e., "self-initiated surface graft polymerization" successfully prepared the surface with controlled graft layer thickness and density. This simple self-initiated surface graft polymerization would be highly suitable for industrial applications as well as the development of medical devices. The synthesis of a self-initiated biocompatible polymer having unique properties such as anti-protein adsorption and wettability by the photoinduced grafting-from polymerization reaction is a novel phenomenon in the field of biomaterials and bioengineering sciences, and the fabrication of the PMPC-grafted PEEK surface can result in the development of next-generation multifunctional biomaterials.

5. Conclusions

A biocompatible and highly hydrophilic nanometer-scale modified surface was successfully fabricated on the PEEK substrate by the photo-induced graft polymerization of PMPC in the absence of photo-initiators, i.e., "self-initiated surface graft polymerization." Since MPC is a highly hydrophilic compound, the water wettability and lubricity of the PMPC-grafted PEEK surface were greater than that of the untreated PEEK surface due to the formation of a PMPC nanometer-scale layer. In addition, the amount of BSA adsorbed on the PMPC-grafted PEEK surface considerably decreased compared to that in the case of untreated PEEK. The density and thickness of the grafting layer could be controlled by the photo-irradiation time and monomer concentration.

References

1. Ishihara K, Nomura H, Mihara T, Kurita K, Iwasaki Y, Nakabayashi N, *J Biomed Mater Res* 1998, **39**, 323-330.
2. Ishihara K, Ziats NP, Tierney BP, Nakabayashi N, Anderson JM, *J Biomed Mater Res* 1991, **25**, 1397-1407.
3. Ishihara K, Oshida H, Ueda T, Endo Y, Watanabe A, Nakabayashi N, *J Biomed Mater Res* 1992, **26**, 1543-1552.
4. Kyomoto M, Ishihara K, *ACS Appl Mater Interfaces* 2009, **1**, 537-542.
5. Kyomoto M, Moro T, Takatoti Y, Kawaguchi H, Nakamura K, Ishihara K, *Biomaterials* 2010, **31**, 1017-1024.
6. Ishihara K, Ueda T, Nakabayashi N, *Polym J* 1990, **22**, 355-360.
7. He D, Susanto H, Ulbricht M, *Prog Polym Sci* 2009, **34**, 62-98.
8. Kyomoto M, Moro T, Konno T, Takamada H, Yamawaki N, Kawaguchi H, Nakamura K, Ishihara K, *J Biomed Mater Res A* 2007, **82**, 10-17.
9. Kyomoto M, Moro T, Iwasaki Y, Miyaji F, Kawaguchi H, Takatori Y, Nakamura K, Ishihara K, *J Biomed Mater Res A* 2009, **91**, 730-741.
10. Matsuda T, Kaneko M, Ge S, *Biomaterials* 2003, **24**, 4507-4515.
11. Braunecker WA, Matyjaszewsky K, *Prog Polym Sci* 2007, **32**, 93-146.
12. Kyomoto M, Moro T, Miyaji F, Hashimoto M, Kawaguchi H, Takatori Y, Nakamura K, Ishihara K, *J Biomed Mater Res A* 2008, **86**, 439-447.
13. Ishikawa Y, Hiratsuka K, Sasada T, *Wear* 2006, **261**, 500-505.

Biochimica et Biophysica Acta 1810 (2011) 268–275

Contents lists available at ScienceDirect

Biochimica et Biophysica Acta

journal homepage: www.elsevier.com/locate/bbagen

Review

Novel polymer biomaterials and interfaces inspired from cell membrane functions ☆

Kazuhiko Ishihara [a,b,c,d,*], Yusuke Goto [a,c], Madoka Takai [a,c], Ryosuke Matsuno [a,c], Yuuki Inoue [a,d], Tomohiro Konno [b,c,d]

[a] Department of Materials Engineering, School of Engineering, Hongo 7-3-1, Bunkyo-ku, Tokyo 113-8656, Japan
[b] Department of Bioengineering, School of Engineering, Hongo 7-3-1, Bunkyo-ku, Tokyo 113-8656, Japan
[c] Center for NanoBio Integration(CNBI), The University of Tokyo, Hongo 7-3-1, Bunkyo-ku, Tokyo 113-8656, Japan
[d] Core Research Evolution of Science and Technology(CREST), Japan Science and Technology Agency, Sanban-cho 5, Chiyoda-ku, Tokyo 102-0075, Japan

ARTICLE INFO

Article history:
Received 1 December 2009
Received in revised form 6 April 2010
Accepted 16 April 2010
Available online 8 May 2010

Keywords:
Cell membrane
Phospholipid polymer
Biomaterial
Biointerface
Biocompatibility

ABSTRACT

Background: Materials with excellent biocompatibility on interfaces between artificial system and biological system are needed to develop any equipments and devices in bioscience, bioengineering and medicinal science. Suppression of unfavorable biological response on the interface is most important for understanding real functions of biomolecules on the surface. So, we should design and prepare such biomaterials.
Scoop of review: One of the best ways to design the biomaterials is generated from mimicking a cell membrane structure. It is composed of a phospholipid bilayered membrane and embedded proteins and polysaccharides. The surface of the cell membrane-like structure is constructed artificially by molecular integration of phospholipid polymer as platform and conjugated biomolecules. Here, it is introduced as the effectiveness of biointerface with highly biological functions observed on artificial cell membrane structure.
Major conclusions: Reduction of nonspecific protein adsorption is essential for suppression of unfavorable bioresponse and achievement of versatile biomedical applications. Simultaneously, bioconjugation of biomolecules on the phospholipid polymer platform is crucial for a high-performance interface.
General significance: The biointerfaces with both biocompatibility and biofunctionality based on biomolecules must be installed on advanced devices, which are applied in the fields of nanobioscience and nanomedicine. This article is part of a Special Issue entitled Nanotechnologies - Emerging Applications in Biomedicine.

1. Introduction

The cells are surrounded by a cell membrane that helps them adapt to the versatile physiological environment [1,2]. Therefore, the cell membrane is a good candidate for constructing a biointerface platform [3]. Understanding the cell membrane facilitates the engineering of an advanced biointerface with highly controlled properties and functions. Cell membrane formation in nature is highly regulated and finely tuned at the molecular level. Many researches have been reported to construct artificial cells and cell membranes by molecular assembly method. Phospholipid bilayered membrane is used as a platform and some proteins and other biomolecules are embedded in the membrane. Also, the structure has been constructed by Langmuir–Blodgett method with various phospholipid molecules. There researches provide suitable model to understand cell membrane functions [4–7].

Preparation of artificial cell membrane structure composed of phospholipid polymer and biomolecules has been paid much attention to obtain excellent biofunctions [8–12]. Basically, the polymers having phospholipid polar group and phosphorylcholine group, were synthesized and functionalized by changing the molecular structure of the polymer [13,14]. Fundamental researches have been carried out to clarify the potential of biocompatibility of the phospholipid polymers [15–17]. For example, many implantable medical devices coated with phospholipid polymer are applied clinically and in the stage of clinical trials [18–21]. We also prepared nanobiodevices covered with the artificial cell membrane composed of phospholipid polymer platform and immobilized biomolecules on it [22,23]. In this review, design of biomaterials with artificial cell membrane structure and the importance of interface between materials and biological system will be represented.

2. Polymers bearing phospholipid polar group as biomaterials

2.1. Molecular design of phospholipid polymers

The fundamental strategy of a bioinspired approach is to clearly understand the principles of the cell membrane functions. Fig. 1 shows the typical illustration of a cell membrane along with some

☆ This article is part of a Special Issue entitled Nanotechnologies - Emerging Applications in Biomedicine.

* Corresponding author. Department of Materials Engineering, Hongo 7-3-1, Bunkyo-ku, Tokyo 113-8656, Japan. Tel.: +81 3 5841 7124; fax: +81 3 5841 8647.
E-mail address: ishihara@mpc.t.u-tokyo.ac.jp (K. Ishihara).

0304-4165/$ – see front matter
doi:10.1016/j.bbagen.2010.04.008

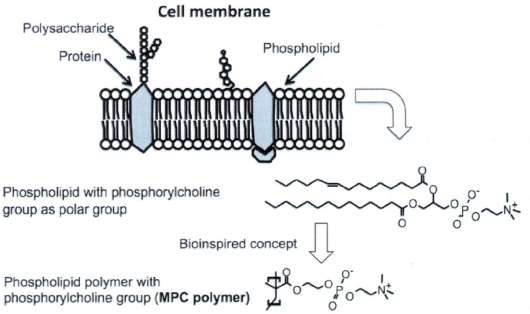

Fig. 1. Schematic representation of cell membrane.

functions. Numerous biomolecules are embedded in the phospholipid bilayer, e.g., antibodies, glycoproteins, enzymes, and receptors. The favorable biofunctions are inertness of the capsule, biological affinity, enzymatic reaction, etc. These are fundamental biomolecules that play important roles. In the bioinspired approach, molecular components were assembled to perform these selected biofunctions. For example, phospholipids comprise a polar head group and alkyl tail groups. However, surface enrichment of phospholipid polar groups is essential for preparing the biointerface. In other words, the entire phospholipid molecules are not necessary for formation of the biointerface. This is the concept of a fundamental bioinspired approach; we introduce polymer materials to prepare the stable biointerface.

The requirements of establishing ultimate biointerfaces are (i) bioinertness, (ii) easy fabrication, (iii) immobilization of biomolecules under mild condition, (iv) retention of higher biofunctions, and (v) easy accessibility of target molecules without any barrier. We have been utilizing polymers composed of 2-methacryloyloxyethyl phosphorylcholine (MPC), which has phosphorylcholine group in the side chain, as a key material for constructing a biointerface platform. Very recently, some researchers utilized other methacrylates with zwitter ionic polar groups or oligo(ethylene glychol) monomethacrylate for preparing biointerfaces to obtain low fouling surfaces [24–29].

2.2. Biointerfaces composed of the MPC polymers

The biointerface researches with MPC polymers have been conducted worldwide [30–33]. It has opened up new avenues for investigation, particularly in the field of life science research. The MPC allows versatile polymerization techniques with appropriate comonomers: conventional radical, living radical and atom transfer radical polymerizations. Therefore, precisely designed MPC polymers have been easily synthesized; herein, the ultimate biointerfaces by the MPC polymer is introduced along with recent excellent results. The synthesized MPC polymers are used in various forms such as polymer solution, hydrogel, polymer-coated surface, polymer-grafted surface, and nanoparticles. In particular, hydrophilic MPC unit and hydrophobic *n*-butyl methacrylate (BMA) unit are of great importance for the fabrication of high-performance biointerfaces. The best monomer unit fraction in the copolymer for coating on the medical devices was reported to be 0.3 of the MPC unit and 0.7 of the BMA unit; moreover, the molecular weight of the copolymer should be controlled to above 5×10^5 [9,11]. The MPC polymer-coated surface serves double functions—suppression of nonspecific protein adsorption from the living organism and processing of robust polymer coating. On the surface treated with the MPC polymer, the phosphorylcholine groups in the MPC unit were enriched in the outermost surface of the substrate relative to the inner side of the substrate [34,35]. The plausible mechanism for the suppression of nonspecific protein adsorption was discussed in terms of water structure on the surface. Enrichment of the phosphorylcholine groups provided a higher free water fraction on the polymer-coated surface, and it strongly suppressed protein adsorption by release of bound water molecules on the protein surface. [36–39].

Based on the chemical structure of the poly(MPC-*co*-BMA), which provides excellent anti-biofouling surface, the new polymers are designed to conjugate biomolecules on the surface under mild conditions. The reaction for conjugation of biomolecules must be carried out in an aqueous medium with physiological pH range and temperature due to low stability of biomolecules. So, active ester groups and phenylboronic acid group are useful for reacting with amino group and sugar units in the biomolecules, respectively.

As shown in Fig. 2, a polymer composed of MPC, BMA, and *p*-nitrophenyloxycarbonyl poly(oxyethylene)methacrylate (MEONP) units (the polymer is named as PMBN) was designed and prepared for obtaining excellent biointerfaces [40,41]. These three monomer units show unique chemical and biological functions. One of the bioconjugate functions was the incorporation of an active ester group on MEONP. The active ester group was connected to the methacrylate via the oxyethylene spacer [42]. The length of the oxyethylene spacer can be changed with the use of appropriate precursors. The spacer length was changed from 0.5 to 2 nm, and the location of the immobilized biomolecules was also changed. The phosphorylcholine groups were at the position of 0.4 nm from the substrate, which was calculated by the molecular structure of the MPC unit. We found that the durability of the immobilized biomolecules depended on the spacer length, by changing the number of repeating units of the oxyethylene group in MEONP. The spacer length played a key role in reducing background signals in γ-globulin (IgG)-immobilized biosensing. Biomolecules containing amino groups could couple to the ester groups on the polymer backbone under physiological conditions, producing *p*-nitrophenol as a leaving group. The bioconjugate reaction is accelerated under neutral or weak alkaline conditions (pH 7.4–8.0). By this polymer, PMBN, the biomolecules could immobilize in the platform of phosphorylcholine group-enriched surface the same as cell membrane surfaces. Also, it could be prepared from nano-scaled structure using PMBN on the surface of electrode by electrospray deposition (ESD) method to enlarge surface area for conjugation of biomolecules. Much amount of biomolecules could be immobilized on the ESD-surface compared with that on plane spin-coated surface [43].

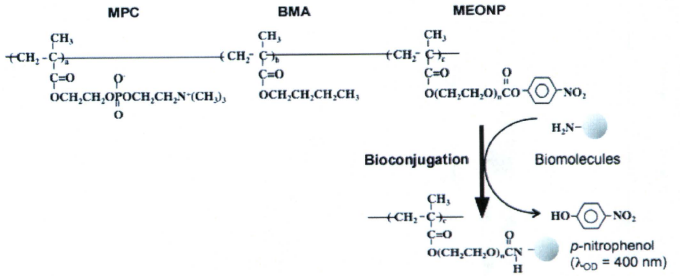

Fig. 2. Chemical structure of phospholipid polymer, poly(MPC-*co*-BMA-*co*-MEONP) (PMBN) for bioconjugation based on artificial membrane structure.

3. Polymer nanoparticles with artificial cell membrane surface

3.1. Preparation of polymer nanoparticles

We focus on monodispersed nanoparticles as one of the biointerfaces, and introduce affinity separation, sensing, and diagnosis. The PMBN was easily enriched onto the nanoparticle surface by the solvent evaporation method. We first succeeded in preparing monodispersed nanoparticles covered with water-soluble and amphiphilic poly(MPC-*co*-BMA) (PMB30W: mole fraction of MPC unit in the polymer is 0.30). The PMB30W aqueous solution provided hydrophobic domains by aggregation of the polymer chain [44]. This is the fundamental driving force for the reduction of surface free energy (water–methylene chloride interface) to stabilize methylene chloride droplets involved in the formation of other polymers such as poly(lactic acid) (PLA) and polystyrene. Moreover, Konno et al. first developed monodispersed PLA nanoparticles covered with PMBN (PMBN/PLA-NP) [45]. The phosphorylcholine groups in the MPC unit and active ester groups in the MEONP groups were enriched in the outermost surface; evidence for this was obtained by X-ray photoelectron spectroscopy. The average diameters of the PMBN/PLA-NP ranged from 250 nm to 300 nm as shown in Fig. 3. The zeta-potential of the PLA surface was a large negative value about −60 mV, however, that of the PMBN/PLA-NP became to ranged from −6.8 mV to −2.0 mV. This is because of the electrical neutrality of the phosphorylcholine groups due to the formation of an inner salt between phosphate anions and trimethylammonium cations. The appropriate materials that can be used as nanoparticle cores are polymers, metals, and ceramic. In particular, PMBN enables coating of the particle surface; thus, titanium oxide and silica nanoparticles are easily coated by PMBN. Active ester groups were located on the nanoparticles, and the typical surface concentration was evaluated to be 1.0 nmol per mg of polystyrene nanoparticles (PS-NP). The bioconjugation was achieved simultaneously as well as continuously. Moreover, multiple biomolecules could be immobilized via the active ester groups [46–48]. We observed that multiple immobilizations of proteins on the PMBN-coated nanoparticles were achieved. Considering this, PMBN comprising phosphorylcholine and active ester groups is of great importance as a platform for a high-performance biointerface facilitating affinity separation, sequential reaction, and biomolecular detection.

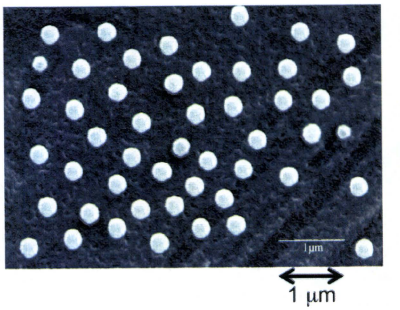

Fig. 3. Electron microscopic picture of polymer nanoparticles covered with artificial cell membrane.

3.2. Binding of target biomolecules on nanoparticles based on bioreaction

Nonselective adsorption of biomolecules on the surface makes noise for sensing of target molecules. The MPC polymer can suppress protein adsorption significantly. The effects of the phosphorylcholine groups on the adsorption of bovine serum albumin (BSA) to the nanoparticles were evaluated [49]. To avoid chemical reaction with BSA, the active ester groups on PMBN/PLA-NP were reacted with glycine for blocking the active ester groups in this experiment. Fig. 4

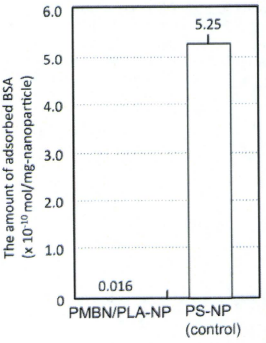

Fig. 4. Amount of BSA adsorbed on polymer nanoparticles without and with artificial cell membrane surface.

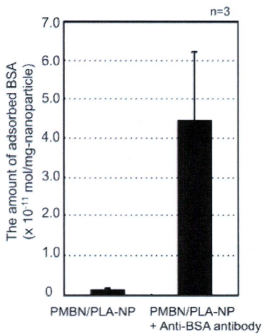

Fig. 5. Amount of BSA captured on polymer nanoparticles immobilized anti-BSA antibody based on antigen–antibody reaction.

shows the amount of BSA adsorbed on various nanoparticles. Numerous BSA molecules were adsorbed on the commercially available PS-NP whereas these molecules were hardly adsorbed on the glycine-reacted PMBN/PLA-NP; the value was approximately 1/300 as compared with that on PS-NP. The surface of PS-NP was hydrophobic and adsorbed proteins. PMBN/PLA-NP was suitable for developing affinity nanoparticles because of their considerable ability to prevent nonspecific adsorption.

The activity and function of the antibody immobilized on the PMBN/PLA-NP were evaluated by observing the antigen–antibody reaction (Fig. 5). The amount of BSA on the anti-BSA antibody-immobilized PMBN/PLA-NP was higher than that on PMBN/PLA-NP without antibody immobilization. This result indicates that the amount of BSA increased by reacting with the antibody immobilized on the surface of PMBN/PLA-NP. Based on this result, the antibody-immobilized PMBN/PLA-NP could function as affinity nanoparticles. The dissociation constant (Kd) of the antigen/antibody complex substantially defines the performance of affinity-based separation, diagnosis, and detection systems. To evaluate the performance of PMBN/PLA-NP as an affinity nanoparticle, the dissociation constant of the antigen/antibody complex on PMBN/PLA-NP was measured [49]. The dissociation constant could be calculated from these plots, and it was observed to be 2.7×10^{-7} M for the anti-BSA antibody-immobilized PMBN/PLA-NP (PMBN/PLA/anti-BSA-NP) and 1.3×10^{-5} M for the anti-BSA antibody-immobilized PS-NP modified with succinimide moiety (PS-suc-NP) on the surface (PS/anti-BSA-NP). Thus, the affinity of the anti-BSA antibody to BSA observed on the PMBN/PLA/anti-BSA-NP was approximately 200-fold higher than that on the PS/anti-BSA-NP. The K_d value generally ranges from 10^{-7} to 10^{-10} for an antigen–antibody complex [50]. The K_d value of the anti-BSA antibody immobilized on PMBN/PLA-NP for BSA is considered valid while that for the anti-BSA antibody immobilized on PS-suc-NP is higher than the reported value. This indicates that the antibody immobilized on the PMBN/PLA-NP had a strong affinity toward the antigen, maintaining the activity of the antibody even when immobilized on the nanoparticles. However, in the case of antibodies immobilized on the PS-suc-NP, a large K_d value was observed; this was due to a weakening in the affinity for the antigen by denaturation of the antibody during immobilization. These results indicate the effects of the phosphorylcholine groups in preventing the denaturation of the antibody.

4. Specific cellular uptake of nanoparticles covered with artificial cell membrane conjugated with specific biomolecules

4.1. Preparation of polymer nanoparticles embedding fluorescence marker

Semiconductor nanocrystalites (quantum dots or QDs) have gained much interest as a promising alternative to organic dyes for biological imaging. QDs ranging in size between 2 nm and 6 nm have unique optical properties: material- and size-dependent emission spectra, a wide absorption spectrum, high quantum yields, simultaneous multicolor emissions, and especially excellent resistance to photobleaching. This photostability is a critical feature in most fluorescence applications, particularly for long-term monitoring of labeled substances, and is an area in which QDs have a singular advantage over organic dyes. As QDs themselves are hydrophobic, the key to developing QDs as a tool in biological systems is to achieve good dispersion ability in an aqueous medium, and compatibility with biological components including cells [51–53].

Polymer nanoparticles embedding QDs covered with PMBN (PMBN/PLA/QD) were designed by making an assembly of phosphorylcholine groups as platform and biomolecules immobilized on the surface of nanoparticles (Fig. 6) [54]. In spite of numerous efforts [55,56], the problems of cytotoxicity and the nonselective cellular uptake of QDs remain. As mentioned above, the PMBN/PLA-NPs show the bioinert abilities and they may avoid phagocytosis from macrophage-like cells [57]. That is, the phosphorylcholine group coverings suppress nonspecific interactions between bulk materials and cell, and create a specific affinity by ligand molecules immobilized on the surface.

4.2. Cellular uptake of the PMBN/PLA/QD

We observed that PMBN/PLA/QD had the abilities to highly resist nonselective cellular uptake from HeLa cells and to permeate the membrane of HeLa cells effectively when arginine octapeptide (R8)

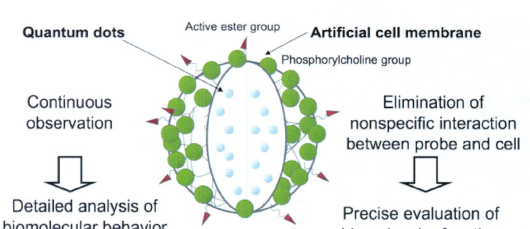

Fig. 6. Schematic representation of polymer nanoparticles embedding QD with artificial cell membrane surface.

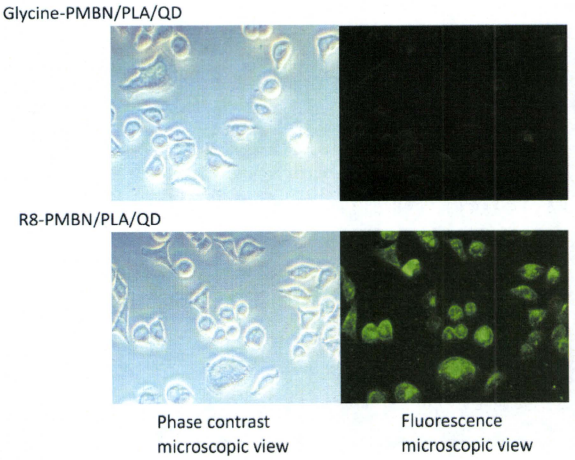

Fig. 7. Uptake of polymer nanoparticles covered with artificial cell membrane without and with R8 immobilization.

was immobilized on the surface of the nanoparticles as shown in Fig. 7 [54]. The R8 is well known as cell membrane penetrating peptide (CPP), so its specific functions are observed with the polymer nanoparticles. In Fig. 8, a plot of the intensity of each PMBN/PLA/QD in cells versus incubation time shows that glycine-masked PMBN/PLA/QD (glycine–PMBN/PLA/QD) completely suppresses the nonselective uptake from HeLa cells. We also confirmed that no glycine–PMBN/PLA/QD was uptaken by HeLa cell even after incubation for 24 h. In general, conventional nanoparticles can be uptaken by the cells without any selectively [57]. Thus, this result indicated that our PMBN/PLA/QD can obtain high signal to noise ratio compared with other imaging probes because there is no background fluorescence caused by nonselective uptake of imaging probes. On the other hand, R8-conjugated PMBN/PLA/QD internalized effectively into cells. The uptake of R8–PMBN/PLA/QD significantly increased within first 15 min, but the uptake rate gradually slowed and reached a plateau at 1 h. However, we cannot obtain from only this information where R8–PMBN/PLA/QD located in the cell at each time. Thus, further research about the location of R8–PMBN/PLA/QD was required.

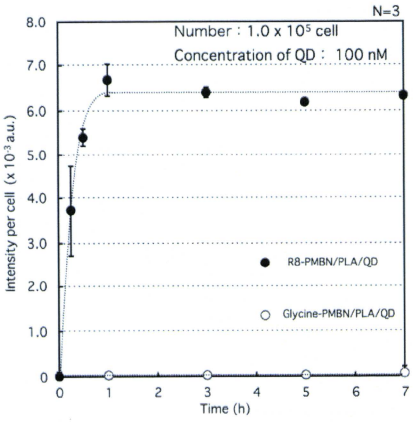

Fig. 8. Time dependence of cellular uptake of polymer nanoparticles. Closed plots: glycine–PMBN/PLA/QD, open plots: R8–PMBN/PLA/QD.

For determining the location of R8–PMBN/PLA/QD at each time, HeLa cells incubated with R8–PMBN/PLA/QD was observed by a confocal laser scanning microscopy (CLSM). Fig. 9 shows that R8–PMBN/PLA/QD attached immediately to the cell membrane within first 5 min and began to internalize into endosome at 15–30 min. The amount of internalized R8–PMBN/PLA/QD increased at 1–3 h and whole R8–PMBN/PLA/QD which attached to cell membrane entered into endosome in 5 h. These results revealed the kinetic behavior of R8-mediated internalization into the cell. Several lines of evidences demonstrated that the PMBN/PLA/QD is a most suitable analytic tool for kinetic analysis of biomolecules.

4.3. The evaluation of the inflammatory response induced by PMBN/PLA/QD

It was reported that PMBN/PLA/QD have no cytotoxicity for 3 days even after internalization in HeLa cells [51]. However, there are some possibilities of the induction of inflammation reaction even when no cytotoxicity appears. Thus, more studies are required with respect to the inflammatory response.

Mouse macrophage RAW264.7 cell, known for its sensitivity to inflammatory response, was used as a model system. RAW264.7 cell was incubated with PMBN/PLA/QD for 24 h. After incubation, the inflammatory response was measured by using real-time reverse transcription polymerase chain reaction (RT-PCR). Oligonucleotides TNF-α-F (5′-GAGCAGCTGGAGTGGCTGCTGAG-3′) and TNF-α-R (5′-

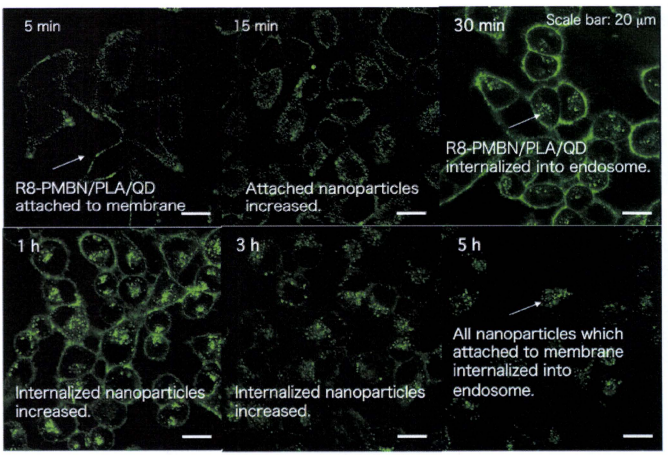

Fig. 9. LCMS analysis of internalization of R8–PMBN/PLA/QD.

TAGACCTGCCCGGACTCCGC-3′) were used for detection of tumor necrosis factor-alpha (TNF-α); GAPDH-F (5′-AATGTGTCCGTCGTGGAT CT-3′) and GAPDH-R (5′-CCCTGTTGCTGTAGCCG TAT-3′) were used for glyceraldehydes-3-phosphate dehydrogenase (GAPDH). The expression of TNF-α mRNA was standardized as the relative value to that obtained for GAPDH mRNA. As negative and positive controls, a normal cell and the cell with 100 ng/mL lipopolysaccharide were used respectively. Fig. 10 shows the relative expression of TNF-α mRNA to GAPDH mRNA in RAW264.7 cells incubated with R8 or glycine–PMBN/PLA/QD for a day. No significant difference between negative control and PMBN/PLA/QDs in the expression of TNF-α mRNA was observed. This indicated that phosphorylcholine groups on the surface of PMBN/PLA/QD suppress the inflammatory reaction in RAW264.7 cells even when internalizing into cells due to the ologopeptide. From these findings, our PMBN/PLA/QD can eliminate the unwished interactions between probes themselves and cell, such as a nonselective cellular uptake, cytotoxicity and inflammation response.

4.4. The assessment of the abilities of various octapeptides as a cell membrane penetration peptide

Many research groups reported that arginine-rich peptide is useful as a CPP [58,59]. However, the abilities of other oligopeptides to penetrate the cell membrane have not been well characterized. Thus, we evaluated the function of various octapeptides as a CPP by using our PMBN/PLA/QD as an analyzing tool. To assess the main factor

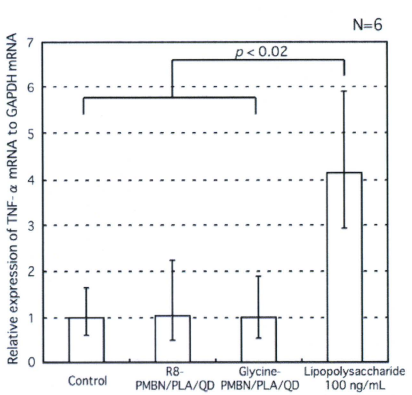

Fig. 10. Relative expression of TNF-α mRNA to GAPDH mRNA in RAW264.7 cells incubated with polymer nanoparticles.

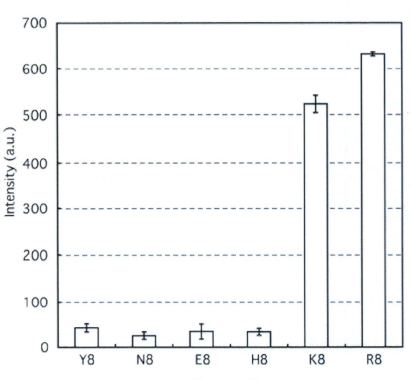

Fig. 11. Effect of amino acid residue of immobilized oligopeptide on cellular uptake.

determining the abilities of oligopeptides as a CPP, we selected various octapeptides that consist of one kind of amino acid (octa-tyrosine (Y8: hydrophobic), octa-asparagine (N8: hydrophilic), octa-glutamic acid (E8: hydrophilic and anionic), octa-histidine (H8: hydrophilic and weakly cationic), octa-lysine (K8: hydrophilic and cationic), or octa-arginine (R8: hydrophobic and cationic)). These peptides were conjugated with PMBN/PLA/QD respectively. A HeLa cell (seeded into 12-well plates at 1.0×10^4 cell/well in 1 mL of culture medium) was incubated with each octapeptide-conjugated PMBN/PLA/QD for 5 h. The quantification of the uptake of PMBN/PLA/QD was performed. As shown in Fig. 11, only K8 and R8 conjugated PMBN/PLA/QD could internalize in HeLa cells. This result indicated that the hydrophilic and cationic nature of oligopeptides play a key role in the cell membrane permeation. In order to understand the mechanism of cell penetration induced by these hydrophilic and cationic oligopeptides, it will be required to investigate the relationship between surface cationic density on the nanoparticles and cell membrane permeation.

5. Conclusion

Many important applications of nanotechnology would not be achievable without proper design of nanosturcture. As integrative field of biomedical nanotechnology evolves, more systematic approaches for the chemical design of nanostructures will be required. Furthermore, as the researchers start to construct multifunctional nanostructures, the interface between nanostructure and biological environments will be critical. In this study, our artificial cell membrane–biointerface can provide the imaging probes with the abilities to suppress completely the interactions between imaging probes themselves and cells. This biointerface is necessary to study the fundamental information of the biomolecular behavior in cellular environments. We described the kinetic behavior in cytoplasm of our polymer nanoparticles containing QDs with artificial cell membrane–biointerface. Although these nanoparticles can avoid the nonselective cellular uptake from mammalian cells, when bioactive molecules were immobilized, our nanoparticles can provide the various information about the specific interaction between biomolecules and cells. From these findings, we conclude that the nanoparticles are candidates for the role of stable and highly sensitive fluorescent bioimaging probes in the fields of nanotechnology. Controlling interactions with cells is receiving considerable importance in biomedical fields, including nanobioengineering and cell and tissue engineering. The bioinspired interfaces described here are a promising design for revealing a universal platform that integrates polymer chemistry; material science; and engineering, biochemistry, cell biology, and nanofabrication.

Acknowledgements

This research was partially supported by Special Coordination Funds for Promoting Science and Technology from the Ministry of Education, Culture, Sports, Science, and Technology, Japan.

References

[1] S.J. Singer, G.L. Nicholson, The fluid mosaic model of the structure of cell membranes, Science 175 (1972) 720–731.
[2] P.L. Yeagle, The Membranes of Cells, second ed.Academic Press, New York, 1993.
[3] J.A. Hayward, D. Chapman, Biomembrane surfaces as models for polymer design: the potential for haemocompatibility, Biomaterials 5 (1984) 135–142.
[4] J.J. Ramsden, G.I. Bachmanova, A.I. Archakov, Immobilization of proteins to lipid bilayers, Biosens. Bioelectron. 5 (1996) 523–528.
[5] X.L. Sun, W. Cui, T. Kai, E.L. Chaikof, A facile synthesis of bifunctional phospholipids for biomimetic membrane engineering, Tetrahedron 60 (2004) 11765–11770.
[6] L. Brunsveld, H. Waldmann, D. Huster, Membrane binding of lipidated Ras peptides and proteins—the structural point of view, Biochim. Biophys. Acta 1788 (2009) 273–288.
[7] H.M. Cho, D.Y. Cho, J.Y. Jeon, S.Y. Hwang, I.S. Ahn, J. Choo, E.K. Lee, Fabrication of protein-anchoring surface by modification of SiO_2 with liposomal bilayer, Colloids Surf. B: Biointerfaces 75 (2010) 209–213.
[8] K. Ishihara, J. Watanabe, Y. Iwasaki, Bioinspired polymer surfaces for prevention of bioresponse, Mater. Sci. Forum 426–432 (2003) 3171–3176.
[9] J. Watanabe, J.-W. Park, T. Ito, M. Takai, K. Ishihara, Biofunctionalization of phospholipid polymer nanoparticles, in: C.S.S.R. Kumar (Ed.), Nanotechnologies for the Life Science, Biofunctionalizaation of Nanomaterials, vol. 1, Wiley-VCH, Weinheim, 2005, pp. 125–149.
[10] J. Watanabe, K. Ishihara, Biointerface, bioconjugation, and biomatrix based on bioinspired phospholipid polymers, in: H.S. Nalwa (Ed.), Handbook of Nanostructured Biomaterials and Their Applications in Nanobiotechnology vol. 1, American Scientific Publishers, 2005, pp. 129–165.
[11] J. Watanabe, K. Ishihara, Establishing ultimate biointerfaces covered with phosphorylcholine groups, Colloids Surf. B: Biointerfaces 65 (2008) 155–165.
[12] K. Ishihara, K. Nishizawa, Y. Goto, M. Takai, Bioinspired polymer surfaces for nanodevices and nanomedicine, Adv. Sci. Technol. 57 (2008) 5–14.
[13] K. Ishihara, T. Ueda, N. Nakabayashi, Preparation of phospholipid polymers and their properties as polymer hydrogel membrane, Polym. J. 22 (1990) 355–360.
[14] T. Ueda, H. Oshida, K. Kurita, K. Ishihara, N. Nakabayashi, Preparation of 2-methacryloyloxyethyl phosphorylcholine copolymers with alkyl methacrylates and their blood compatibility, Polym. J. 24 (1992) 1259–1269.
[15] K. Ishihara, R. Aragaki, T. Ueda, A. Watanabe, N. Nakabayashi, Reduced thrombogenicity of polymers having phospholipid polar groups, J. Biomed. Mater. Res. 24 (1990) 1069–1077.
[16] K. Ishihara, N.P. Ziats, B.P. Tierney, N. Nakabayashi, J.M. Anderson, Protein adsorption from human plasma is reduced on phospholipid polymers, J. Biomed. Mater. Res. 25 (1991) 1397–1407.
[17] K. Ishihara, H. Oshida, Y. Endo, T. Ueda, A. Watanabe, N. Nakabayashi, Hemocompatibility of human whole blood on polymers with a phospholipid polar group and its mechanism, J. Biomed. Mater. Res. 26 (1992) 1543–1552.
[18] T.A. Snyder, H. Tsukui, S. Kihara, T. Akimoto, K.N. Litwak, M.V. Kameneva, Preclinical biocompatibility assessment of the EVAHEART ventricular assist device: coating comparison and platelet activation, J. Biomed. Mater. Res. A 81 (2007) 85–92.
[19] G.J. Myers, D.R. Johnstone, W.J. Swyer, S. McTeer, S.L. Maxwell, C. Squires, S.N. Ditmore, C.V. Power, L.B. Mitchell, J.E. Ditmore, L.D. Aniuk, G.M. Hirsch, K.J. Buth, Evaluation of mimesys phosphorylcholine (PC)-coated oxygenators during cardiopulmonary bypass in adults, J. Extra-Corpor. Technol. 35 (2003) 6–12.
[20] M. Kyomoto, T. Moro, T. Konno, H. Takadama, N. Yamawaki, H. Kawaguchi, Y. Takatori, K. Nakamura, K. Ishihara, Enhanced wear resistance of modified cross-linked polyethylene by grafting with poly(2-methacryloyloxyethyl phosphorylcholine), J. Biomed. Mater. Res. A 82A (2007) 10–17.
[21] A.L. Lewis, L.A. Tolhurst, P.W. Stratford, Analysis of a phosphorylchline-based polymer coating on a coronary stent pre- and post-implantation, Biomaterials 23 (2002) 1697–1706.
[22] K. Ishihara, M. Takai, Bioinspired interfaces for nanobiodevices based on phospholipid polymer chemistry, J. R. Soc. Interface 6 (2009) S279–S291.
[23] K. Nishizawa, T. Konno, M. Takai, K. Ishihara, Bioconjugated phospholipid polymer biointerface for ELISA, Biomacromolecules 9 (2008) 403–407.
[24] E. Kharlampieva, D. Pristinski, S.A. Sukhishvili, Hydrogen-bonded multilayers of poly(carboxybetaine)s, Macromolecules 40 (2007) 6967–6972.
[25] Y. Chang, S.-C. Liao, A. Higuchi, R.-C. Ruaan, C.-W. Chu, W.-Y. Chen, A highly stable nonbiofouling surface with well-packed grafted zwitterionic polysulfobetaine for plasma protein repulsion, Langmuir 24 (2008) 5453–5458.
[26] Y.-C. Chianga, Y. Changb, A. Higuchia, W.-Y. Chena, R.-C. Ruaana, Sulfobetaine-grafted poly(vinylidene fluoride) ultrafiltration membranes exhibit excellent antifouling property, J. Membr. Sci. 339 (2009) 151–159.
[27] H. Vaisocherová, W. Yang, Z. Zhang, Z. Cao, G. Cheng, M. Piliarik, J. Homola, S. Jiang, Ultralow fouling and functionalizable surface chemistry based on a zwitterionic polymer enabling sensitive and specific protein detection in undiluted blood plasma, Anal. Chem. 80 (2008) 7894–7901.
[28] G. Cheng, G. Li, H. Xue, S. Chen, J.D. Bryers, S. Jiang, Zwitterionic carboxybetaine polymer surfaces and their resistance to long-term biofilm formation, Biomaterials 30 (2009) 5234–5240.
[29] S. Tugulu, H.-A. KlokStability, Nonfouling properties of poly(poly(ethylene glycol) methacrylate) brushes under cell culture conditions, Biomacromolecules 9 (2008) 906–912.
[30] X.-D. Huang, K. Yao, H. Zhang, X.-J. Huang, Z.-K. Xu, Surface modification of silicone intraocular lens by 2-methacryloyloxyethyl phosphoryl-choline binding to reduce *Staphylococcus epidermidis* adherence, Clin. Exp. Ophthalmol. 35 (2007) 462–467.
[31] W. Feng, S. Zhu, K. Ishihara, J.L. Brash, Adsorption of fibrinogen and lysozyme on silicon grafted with, poly(2-methacryloyloxyethyl phosphorylcholine) via surface-initiated atom transfer, radical polymerization, Langmuir 21 (2005) 5980–5987.
[32] S.F. Rose, S. Okere, G.W. Hanlon, A.W. Lloyd, A.L. Lewis, Bacterial adhesion to phosphorylcholine-based polymers with varying cationic charge and the effect of heparin pre-adsorption, J. Mater. Sci. Mater. Med. 16 (2005) 1003–1015.
[33] J.-J. Yuan, A. Schmid, S.P. Armes, Facile synthesis of highly biocompatible poly(2-(methacryloyloxy)ethyl phosphorylcholine)-coated gold nanoparticles in aqueous solution, Langmuir 22 (2006) 11022–11027.
[34] T. Ueda, K. Ishihara, N. Nakabayashi, Adsorption–desorption of proteins on phospholipid polymer surfaces evaluated by dynamic contact angle measurement, J. Biomed. Mater Res. 29 (1995) 381–387.
[35] A. Yamasaki, Y. Imamura, K. Kurita, Y. Iwasaki, N. Nakabayashi, K. Ishihara, Surface mobility of polymers having phosphorylcholine groups connected with various

bridging units and their protein adsorption-resistant properties, Colloids Surf. B: Biointerfaces 28 (2003) 53–62.
[36] K. Ishihara, H. Nomura, T. Mihara, K. Kurita, Y. Iwasaki, N. Nakabayashi, Why do phospholipid polymer reduce protein adsorption? J. Biomed. Mater. Res. 39 (1998) 323–330.
[37] T. Morisaku, J. Watanabe, T. Konno, M. Takai, K. Ishihara, Hydration of phosphorylcholine groups attached to highly swollen polymer hydrogels studied by thermal analysis, Polymer 49 (2008) 4652–4657.
[38] H. Kitano, M. Imai, T. Mori, M. Gemmei-Ide, Y. Yokoyama, K. Ishihara, Structure of water in the vicinity of phospholipid analog copolymers as studied by vibrational spectroscopy, Langmuir 19 (2003) 10260–10266.
[39] D.R. Lu, S.J. Lee, K. Park, Calculation of solvetion interaction energies for protein adsorption on polymer surface, J. Biomater. Sci. Polym. Edn. 3 (1991) 127–147.
[40] K. Takei, K. Konno, J. Watanabe, K. Ishihara, Regulation of enzyme–substrate complexation by phospholipid polymer conjugates for cell engineering, Biomacromolecules 5 (2004) 858–862.
[41] K. Kinoshita, K. Fujimoto, T. Yakabe, S. Saito, Y. Hamaguchi, T. Kikuchi, K. Nonaka, S. Murata, D. Masuda, W. Takada, S. Funaoka, S. Arai, H. Nakanishi, K. Yokoyama, K. Fujiwara, K. Matsubara, Multiple primer extension by DNA polymerase on a novel plastic DNA array coated with a biocompatible polymer, Nucleic Acids Res. 35 (e3) (2007) 1–9.
[42] J. Watanabe, K. Ishihara, Multiple protein immobilized phospholipid polymer nanoparticles: effect of spacer length on residual enzymatic activity and molecular diagnosis, Nanobiotechnology 3 (2008) 76–82.
[43] K. Nishizawa, M. Takai, K. Ishihara, Stabilization of phospholipid polymer surface with three-dimensional; nanometer-scales structure for highly sensitive immunoassay, Colloids Surf. B: Biointerfaces 77 (2010) 263–269.
[44] K. Ishihara, Y. Iwasaki, N. Nakabayashi, Polymeric lipid nanosphere constituted of poly(2-methacryloyloxyethyl phosphorylcholine-co-*n*-butyl methacrylate), Polym. J. 31 (1999) 1231–1236.
[45] K. Konno, J. Watanabe, K. Ishihara, Conjugation of enzymes on polymer nanoparticles covered with phosphorylcholine groups, Biomacromolecules 5 (2004) 342–347.
[46] J. Watanabe, K. Ishihara, Single step diagnosis system using the FRET phenomenon induced by antibody-immobilized phosphorylcholine group-covered polymer nanoparticles, Sens. Actuat. B: Chem. 129 (2008) 87–93.
[47] J. Watanabe, K. Ishihara, Sequential enzymatic reactions and stability of biomolecules immobilized onto phospholipid polymer nanoparticles, Biomacromolecules 7 (2006) 171–175.
[48] T. Ito, J. Watanabe, M. Takai, T. Konno, Y. Iwasaki, K. Ishihara, Dual mode bioreactions on polymer nanoparticles covered with phosphorylcholine group, Colloids Surf. B: Biointerfaces 50 (2006) 55–60.
[49] Y. Goto, R. Matsuno, T. Konno, M. Takai, K. Ishihara, Polymer nanoparticles covered with phosphorylcholine groups and immobilized with antibody for high-affinity separation of proteins, Biomacromolecules 9 (2008) 828–833.
[50] A.A. Garcia, Bioseparation Process Science, Blackwell Science Inc., Cambridge, MA, 1999.
[51] A.M. Smith, H. Duan, A.M. Mohs, S. Ni, Bioconjugated quantum dots for in vivo molecular and cellular imaging, Adv. Drug Deliv. Rev. 60 (2008) 1226–1240.
[52] T. Jamiesona, R. Bakhshia, D. Petrovaa, R. Pococka, M. Imanib, A.M. Seifaliana, Biological applications of quantum dots, Biomaterials 28 (2007) 4717–4732.
[53] A.F.E. Hezinger, J. Teßmar, A. Gopferich, Polymer coating of quantum dots—a powerful tool toward diagnostics and sensorics, Eur. J. Pharm. Biopharm. 68 (2008) 138–152.
[54] Y. Goto, R. Matsuno, T. Konno, M. Takai, K. Ishihara, Artificial cell membrane-covered nanoparticles embedding quantum dots as stable and highly sensitive fluorescence bioimaging probes, Biomacromolecules 9 (2008) 3252–3257.
[55] X. Wu, H. Liu, J. Liu, K.N. Haley, J.A. Treadway, J.P. Larson, N. Ge, F. Peale, M.P. Bruchez, Immunofluorescent labeling of cancer marker Her2 and other cellular targets with semiconductor quantum dots, Nat. Biotechnol. 21 (2003) 41–46.
[56] B. Dubertret, P. Skourides, D.J. Norris, V. Noireaux, A.H. Brivanlou, A. Libchanber, In vivo imaging of quantum dots encapsulated in phospholipid micelles, Science 298 (2002) 1759–1762.
[57] T. Moro, Y. Takatori, K. Ishihara, T. Konno, Y. Takigawa, T. Matsushita, U.I. Chung, K. Nakamura, H. Kawaguchi, Surface grafting of artificial joints with a biocompatible polymer for preventing periprosthetic osteolysis, Nat. Mater. 3 (2004) 829–836.
[58] I.A. Khalil, K. Kogure, S. Futaki, S. Hama, H. Akita, M. Ueno, H. Kishida, M. Kudoh, Y. Mishima, K. Kataoka, M. Yamada, H. Harashima, Octaarginine-modified multifunctional envelope-type nanoparticles for gene delivery. Gene Ther. 14 (2007) 682–689.
[59] A. El-Sayed, I.A. Khalil, K. Kogure, S. Futaki, H. Harashima, Octaarginine- and octalysine-modified nanoparticles have different modes of endosomal escape, J. Biol. Chem. 283 (2008) 23450–23610.